Ground-state energy anisotropy for directed polymers in random media

1998 J. Phys. A: Math. Gen. 31 5939

(http://iopscience.iop.org/0305-4470/31/28/009)

J. Phys. A: Math. Gen. **31** (1998) 5939–5952. Printed in the UK PII: S0305-4470(98)93090-6

Ground-state energy anisotropy for directed polymers in random media

Joachim Krug† and Timothy Halpin-Healy‡

† Fachbereich Physik, Universität GH Essen, D-45117 Essen, Germany

‡ Physics Department, Barnard College, Columbia University, New York, NY 10027-6598, USA

Received 2 April 1998

Abstract. The orientation dependence of the line energy of zero-temperature directed polymers is studied analytically and numerically for the two-dimensional square lattice with site disorder. Using the equivalence to single-step growth models, the exact line energy of maximum energy paths is computed for exponential and geometric disorder distributions. The resulting expression depends on the distributions only through their mean and variance. A universal square-root singularity appears in the ground-state energy as the line orientation approaches the edges of the wedge-shaped lattice. We also discuss the relationship between point-to-point and point-to-line optimization problems, as well as their connection to the classic Wulff construction for crystal shapes. In addition, we derive some general, distribution-independent properties of the optimal path angle in the point-to-line configuration. This angle is argued to be directly measurable in fracture experiments of anisotropic materials such as paper.

1. Introduction

Surface and interface energies in crystalline solids are anisotropic owing to the lattice structure. Through the celebrated Wulff construction [1], this anisotropy is expressed in the equilibrium crystal shape. Using the methods of statistical mechanics to compute the orientation-dependent interface free energy, it is therefore possible in principle to predict the shape of macroscopic crystals from microscopic models [2]. In practice, this programme has been carried out only for simple cases such as domain shapes in the two-dimensional Ising model [3].

During the past decade, it has become widely appreciated that the properties of interfaces are strongly affected by energetic or structural disorder [4]. A paradigmatic system is the two-dimensional Ising model with bond disorder first studied by Huse and Henley [5]. Since interfaces in two dimensions are directed lines, this problem is equivalent to a *directed polymer in a random medium* (DPRM) [6]. Mappings to a variety of other equivalent representations [7] have led to a detailed understanding of the fluctuation properties of the $(1 + 1)$-dimensional DPRM [8].

Much less is known, however, about the basic *macroscopic* quantity characterizing an interface in a disordered medium, namely, the interface free energy and its orientation dependence [9]. In this paper we provide a detailed study of this question for the $(1 + 1)$-dimensional DPRM. Since interfaces in disordered systems are generally governed by a zero-temperature fixed point [4, 8], the focus is on the *ground-state line energy per unit length*, and the closely related line energy of maximum energy paths. We use the standard square lattice model with paths directed along the diagonal, see figure 1. The conformations

0305-4470/98/285939+14$19.50

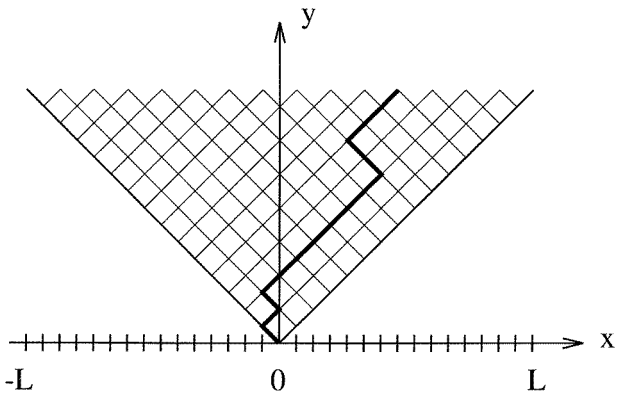

Figure 1. DPRM wedge geometry, with typical L-step directed path.

of the DPRM form a wedge with opening angle $\pi/2$, and the goal is to compute the line energy of maximum and minimum energy paths as a function of the angle $\phi \in [-\pi/4, \pi/4]$ enclosed by the polymer and the lattice diagonal.

The model and the quantities of interest are introduced in the next section. In section 3 we derive a remarkably simple expression for the maximum path energy in the case of exponential and geometric disorder distributions, and we show that maximum and minimum path energies display a universal square root singularity near $\phi = \pm\pi/4$. The analytic predictions are verified through numerical simulations in section 4, and additional results for disorder distributions which cannot be treated analytically are given. In section 5 we consider directed polymers constrained to end at a specified inclined base line, a problem that turns out to be directly related to the Wulff construction, and some conclusions are drawn in section 6.

2. Model and basic quantities

The DPRM lattice used in this work is shown in figure 1. Allowed paths (or polymers) of L steps originate at the apex $(x, y) = (0, 0)$ of the wedge and terminate at one of the $L + 1$ endpoints with coordinates $x = -L, -L + 2, \ldots, L$ and $y = L$. Each site of the lattice carries a random energy $\epsilon(x, y)$. We will adhere to the convention that energies are non-negative, $\epsilon \geqslant 0$, and independently drawn from a probability distribution $P(\epsilon)$ with mean $\bar{\epsilon}$ and variance $\sigma^2 = \bar{\epsilon^2} - \bar{\epsilon}^2$.

The zero-temperature transfer matrix method [5, 8] iteratively generates the restricted ground-state energy $E_{\min}(x, y)$ for all paths ending at (x, y) by solving the recursion relation

$$E_{\min}(x, y+1) = \min[E_{\min}(x-1, y), E_{\min}(x+1, y)] + \epsilon(x, y+1) \qquad (1)$$

with initial condition $E_{\min}(0, 0) = 0$. Similarly the restricted *maximum* path energy $E_{\max}(x, y)$ is obtained from

$$E_{\max}(x, y+1) = \max[E_{\max}(x-1, y), E_{\max}(x+1, y)] + \epsilon(x, y+1). \qquad (2)$$

The interval $[E_{\min}(x, y), E_{\max}(x, y)]$ determines the energy range where the density of states (which contains the full finite-temperature thermodynamic information) is nonzero. Moreover, for a given site energy distribution $P(\epsilon)$ with $\epsilon > 0$, the quantity $-E_{\max}(x, y)$ is the restricted ground-state energy for the corresponding *negative* energy distribution $P(-\epsilon)$, $\epsilon < 0$. For symmetric distributions, $E_{\max}$ and $E_{\min}$ are simply related, see below.

To obtain self-averaging quantities, the path energies are normalized by the path lengths. The Euclidean distance† from the apex to the endpoint (x, L) is $L/\cos\phi$, where $\phi = \arctan(x/L)$ is the angle enclosed by the lattice diagonal. The minimum (ground state) and maximum energies per unit length are therefore defined as

$$\begin{aligned} e_{\min}(\phi) &= \lim_{L\to\infty} L^{-1}\cos\phi\, E_{\min}(\tan\phi L, L) \\ e_{\max}(\phi) &= \lim_{L\to\infty} L^{-1}\cos\phi\, E_{\max}(\tan\phi L, L). \end{aligned} \tag{3}$$

The *average* energy of a path ending at level L is $\bar{\epsilon}L$. The average energy per unit length is therefore $\bar{\epsilon}\cos\phi$, and it follows that

$$e_{\min}(\phi) \leqslant \bar{\epsilon}\cos\phi \leqslant e_{\max}(\phi). \tag{4}$$

The difference between the three quantities in equation (4) is a measure for the amount of optimization involved in finding the ground state. At $\phi = \pm\pi/4$ ($x = \pm L$) only a single allowed path exists, and equation (4) becomes an equality. We also note the identity

$$e_{\min}(\phi) + e_{\max}(\phi) = 2\bar{\epsilon}\cos\phi \tag{5}$$

for symmetric disorder distributions $P(\epsilon)$.

3. Analytic results

Two types of exact results will be derived in this section. First, we show that for the exponential disorder distribution

$$P_0(\epsilon) = \exp(-\epsilon) \tag{6}$$

as well as for the geometric distribution

$$P_p(\epsilon) = \sum_{n=1}^{\infty} p(1-p)^{n-1}\delta(\epsilon - n) \qquad 0 < p < 1 \tag{7}$$

the maximum path energy $e_{\max}(\phi)$ is given by the simple expression

$$e_{\max}(\phi) = \bar{\epsilon}\cos\phi + \sigma\sqrt{\cos 2\phi} \tag{8}$$

in which the disorder distribution enters only through its first and second moments. Since the first term on the right-hand side of (8) is just the average path energy, the second term $\sigma\sqrt{\cos 2\phi}$ represents in a simple way the improvement relative to typical paths achieved in the optimization process.

We will see below in section 4 that equation (8) provides a reasonable approximation also for the uniform disorder distribution, however, in general it is not exact. As a simple counterexample consider the binary distribution

$$P_b(\epsilon) = (1-b)\delta(\epsilon) + b\delta(\epsilon - 1) \qquad 0 < b < 1. \tag{9}$$

Application of (8) yields $e_{\max}(0) = b + \sqrt{b - b^2}$, which exceeds the obvious bound $e_{\max}(0) \leqslant 1$ for $\frac{1}{2} < b < 1$. A plausible interpretation is that $e_{\max}(0)$ sticks to the maximal possible value of unity for $b > \frac{1}{2}$. In fact, this conclusion is qualitatively correct but quantitatively wrong: $e_{\max}(0) = 1$ holds when b exceeds the directed percolation threshold, which is close to 0.7 for site percolation on the square lattice [10].

† We choose the Euclidean path length, rather than the number of steps of a path (which is the same for all paths ending at level y), to be consistent with the continuum viewpoint adopted in the analytic calculations.

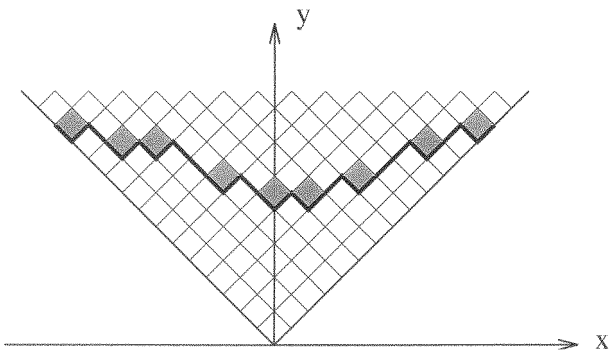

Figure 2. DPRM's close kinetic roughening relation: single-step model. Shaded diamonds indicate legal growth events.

The second exact result concerns the behaviour of $e_{\min}$ and $e_{\max}$ near the edges of the wedge, at $\phi = \pm\pi/4$. We will show in section 3.2 that the square-root singularity

$$|e_{\max}(\phi) - \bar{\epsilon}/\sqrt{2}| \sim |\phi \mp \pi/4|^{1/2} \qquad \phi \to \pm\pi/4 \tag{10}$$

appearing in the expression (8) is a generic feature of both $e_{\min}$ and $e_{\max}$ for arbitrary disorder distributions, with a prefactor which is proportional to σ.

3.1. The waiting time approach

The two distributions (6) and (7) are singled out because they can be interpreted as *waiting time distributions* for a *Markovian* growth process on the square lattice [11–16]. The process described by the exponential distribution evolves in continuous time, while the geometric distribution corresponds to a stochastic discrete time update where all sites are updated simultaneously and independently with probability p. As a consequence (7) reduces to (6) under $p \to 0$ and a suitable rescaling of energy.

3.1.1. Exponential distribution. The equivalent growth model [12, 14–17] describes the evolution of interface configurations $y = h(x, t)$, which are paths directed along the x-axis and satisfying the single-step constraint $|h(x, t) - h(x + 1, t)| = 1$, see figure 2. Growth, $h(x, t) \to h(x, t) + 2$, occurs at local minima, i.e. sites with $h(x + 1, t) = h(x - 1, t) = h(x, t) + 1$, with independent exponentially distributed waiting times of mean 1. The slope variables $\eta(x, t) = (1 + h(x, t) - h(x + 1, t))/2 \in \{0, 1\}$ then define a totally asymmetric exclusion process [12, 14, 16, 18].

On large scales, the interface shape follows a deterministic hydrodynamic equation of the form

$$\partial_t h = V(\partial_x h) \tag{11}$$

where the inclination-dependent growth rate V is given by [12, 14, 19]

$$V(u) = \tfrac{1}{2}(1 - u^2). \tag{12}$$

The lattice used in our work corresponds to a wedge-shaped initial condition $h(x, 0) = |x|$, which evolves into a self-similar profile

$$h(x, t) = tg(x/t). \tag{13}$$

Inserting this into (11), the shape function $g(\xi)$ has to satisfy

$$g(\xi) - \xi g'(\xi) = V(g'(\xi)) \tag{14}$$

with $g'(\xi) = \mathrm{d}g/\mathrm{d}\xi$. The relevant solution [12] is a parabola,

$$g(\xi) = \tfrac{1}{2}(1 + \xi^2) \qquad \xi \in [-1, 1]. \tag{15}$$

Outside of the 'light cone' $|x| < t$ no growth can take place.

In the mapping between growth models and zero-temperature directed polymers [14–16] the site energies play the role of random waiting times, and the maximum path energy $E_{\max}(x, y)$ becomes the time at which the site (x, y) of the lattice is filled. To compute it, we first express the growth shape in polar coordinates, through a function $\rho(\phi)$ defined by

$$g = \rho(\phi)\cos\phi \qquad \xi = \rho(\phi)\sin\phi. \tag{16}$$

The interface profile at time t is then given by $y = t\rho(\phi)\cos\phi$, $x = t\rho(\phi)\sin\phi$, and the point (x, y) is reached at the time $r/\rho(\phi)$, where $r = \sqrt{x^2 + y^2}$ is the distance to the origin. Comparing this with the definition (3) it follows that

$$e_{\max}(\phi) = 1/\rho(\phi). \tag{17}$$

Inserting (16) into (15) therefore yields a quadratic equation for $e_{\max}$, with the solution

$$e_{\max}(\phi) = \cos\phi + \sqrt{\cos 2\phi} \tag{18}$$

in agreement with equation (8).

3.1.2. Geometric distribution. The discrete time version of the single-step growth model—or rather, the equivalent asymmetric exclusion process—has been studied both in the probabilistic literature [20] and in the context of traffic modelling [21]. The key observation is that in the steady state the local slopes $h(x, t) - h(x + 1, t)$ are distributed as the spins of an Ising chain at finite temperature. As a consequence the inclination-dependent growth rate is given by

$$V(u) = 1 - \sqrt{1 - p + pu^2}. \tag{19}$$

Inserting this into equation (14) it can be verified that the growth shape function is

$$g(\xi) = 1 - \sqrt{(1 - p)(1 - \xi^2/p)}. \tag{20}$$

Transforming to polar coordinates according to (16) and using (17) the expression

$$e_{\max}(\phi) = \frac{1}{p}\left[\cos\phi + \sqrt{(1 - p)\cos 2\phi}\right] \tag{21}$$

for the maximum path energy is obtained, which reduces to the general form (8) by noting that $\bar{\epsilon} = 1/p$ and $\sigma^2 = (1 - p)/p^2$ for the geometric distribution (7).

3.2. The edge singularity

In this section we explain the probabilistic origin of the square-root edge singularity (10). The key arguments were developed previously in the context of queuing theory [22, 23].

To be specific, consider $e_{\min}(\phi)$ near $\phi = \pi/4$. Only a single path ends at $x = L$, and its energy per unit length is $e_{\min}(\pi/4) = \bar{\epsilon}/\sqrt{2}$. The optimal path ending at $x = L - 2$ has a simple structure: it follows the edge $x = y$ up to some level y_s where it shifts to the neighbouring row $x = y - 2$. The position of y_s is chosen to minimize the path energy.

Owing to the one-dimensionality of the path geometry, the typical energy gain thus achieved is proportional to $\sigma\sqrt{L}$ for $L \to \infty$.

Similarly a path ending at $x = L - 2k$ can be described in terms of k switching times $y_s^{(i)}$, $i = 1, \ldots, k$, at which it switches from the row $x = y - 2i + 2$ to the row $y - 2i$. When viewed as a function of the $y_s^{(i)}$, the energy difference between the path ending at $x = L$ and that ending at $x = L - 2k$ traces out a Brownian surface [24] above a k-dimensional substrate space of linear extent L. The minimum height of this surface is proportional to $\sigma\sqrt{L}$ for large L. It follows that, for fixed k [22]

$$\lim_{L\to\infty} \frac{E_{\min}(L, L) - E_{\min}(L - 2k, L)}{\sqrt{L}} = \sigma f(k) \tag{22}$$

where the positive function $f(k)$, related to the extremal properties of k-dimensional Brownian motion with increments of unit variance, is independent of the disorder distribution.

To derive the behaviour of $e_{\min}(\phi)$ near the edge, we would need to simultaneously take $k \to \infty$ and $L \to \infty$ with $2k/L = 1 - \tan\phi$ fixed, and subsequently let $\phi \to \pi/4$. Relying on rigorous support [22, 23] we will assume here that this is equivalent to first taking $L \to \infty$ at fixed k, and then $k \to \infty$ in (22). If the edge singularity is of the form

$$e_{\min}(\phi) = \bar{\epsilon}/\sqrt{2} - C(\pi/4 - \phi)^{\nu} + \mathrm{o}((\pi/4 - \phi)^{\nu}) \tag{23}$$

with $\nu < 1$, equation (3) yields

$$E_{\min}(L, L) - E_{\min}(L - 2k, L) \approx \sqrt{2}LC(\pi/4 - \phi)^{\nu} = \sqrt{2}LC(k/L)^{\nu}. \tag{24}$$

Consistency with (22) then requires $\nu = \frac{1}{2}$ and $f(k) \approx c\sqrt{k}$ for $k \to \infty$, where the constant c is universal (independent of the disorder distribution). Since the argument clearly applies equally well to the maximum energy paths, c can be fixed [23] by comparison with the exact result (8), which yields $C = \sqrt{2}\sigma$ and therefore $c = \sqrt{2}C/\sigma = 2$. We conclude, therefore, that the behaviour of the line energies near $\theta = \pi/4$ is universally given by the expression

$$e_{\min,\max}(\phi) = \bar{\epsilon}/\sqrt{2} \mp \sqrt{2}\sigma|\pi/4 - \phi|^{1/2} + \mathrm{o}(|\pi/4 - \phi|^{1/2}) \tag{25}$$

which depends on the disorder distribution only through its mean and variance.

4. Transfer matrix simulations

As a test of our fundamental expression, equation (8), for the functional form of the disorder-averaged DPRM ground-state energy profile, we have performed extensive numerical simulations of the model in the wedge geometry, as detailed in a recent review paper [8]. In figure 3(a) our results are shown for the exponential and geometric site distributions, ensemble averaging performed over 50 realizations of the random energy landscape for walks in excess of 10^4 steps. For both types of distribution, the agreement is extraordinary; were the simulation data and theory each indicated by full lines, the curves would be indistinguishable to the eye. To give the reader a sense of the quality of the agreement, we have decimated the simulation data sets and used discrete symbols to render the figure more legible. In the case of the exponential distribution, which possesses unit mean and variance, (8) reduces to (18), and we expect a vertical intercept of two. For the even-handed geometric distribution, with $p = \frac{1}{2}$, equation (21) demands an intercept of $2 + \sqrt{2}$. These features, as well as the shape of the profile, are nicely captured by the simulations.

Because of the enticingly simple form, it may be thought that equation (8) has a general applicability that goes beyond those distributions, exponential and geometric, tied to a

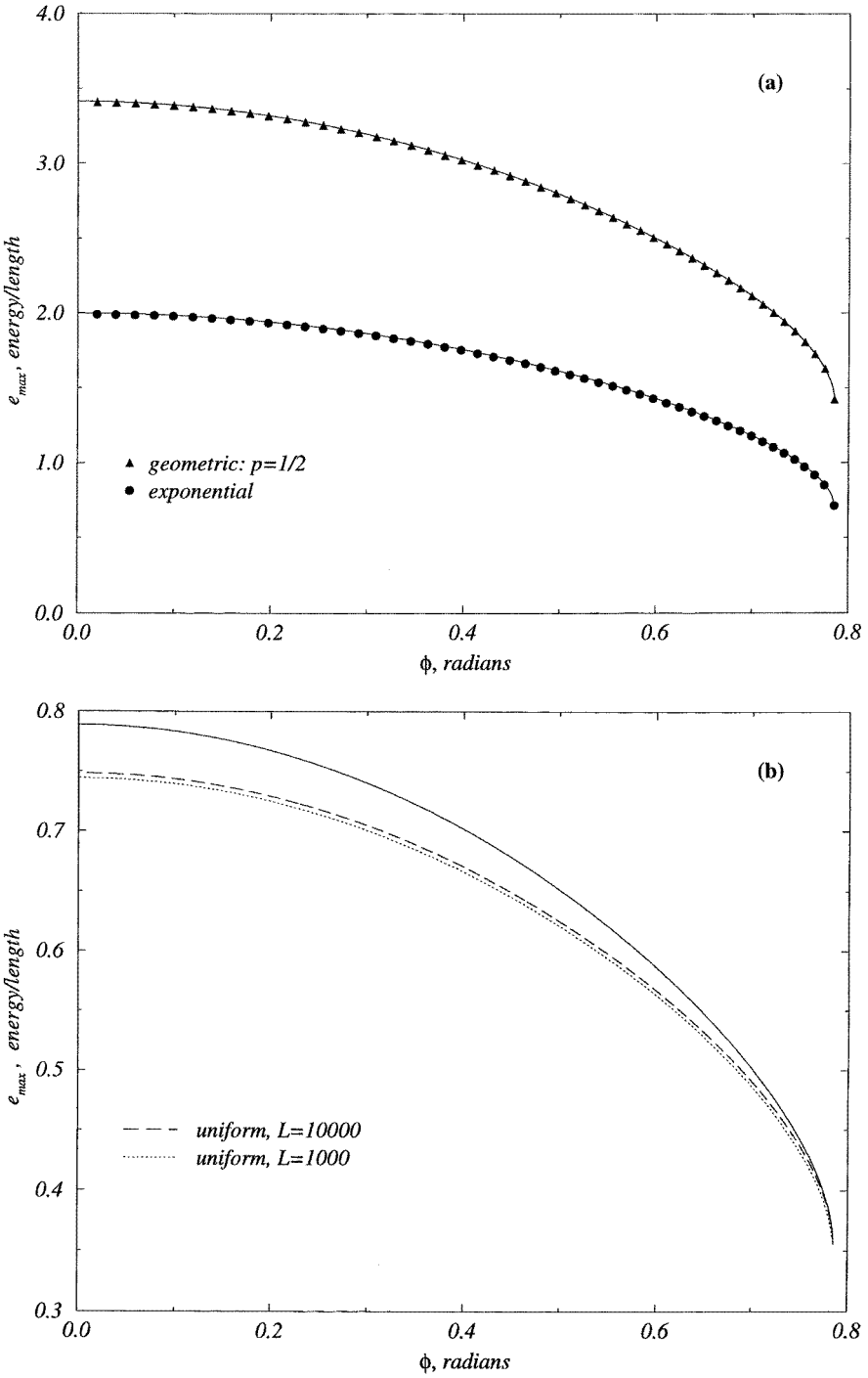

Figure 3. (*a*) Angular dependence of DPRM free-energy profile for exponential and geometric distributions. Full curves indicate exact results, derived in the text, via mapping to the stochastic growth model in waiting time representation. (*b*) Analogous findings for uniform distribution indicates discrepancy between naive 'theoretical' and simulation results, as well as the role of finite-size effects.

waiting-time description of Markovian dynamics. As discussed above, this is not the case. Even so, the discrepancy while undeniable, is quite small, at least for the case of the uniform distribution, see figure 3(*b*). There, we plot results for systems with $L = 10^3$ and 10^4, to show the effects of finite system size. Results for $L = 20\,000$, if plotted on the same figure, would be indistinguishable from the broken curve. The full curve is the 'theoretical' result, assuming naive application of equation (8) with mean and variance dictated by the uniform distribution; i.e. $\bar{\epsilon} = \frac{1}{2}$ and $\sigma^2 = \frac{1}{12}$. The disagreement is largest at $\phi = 0$ and is at the 5% level, but vanishes as $\phi \to \pi/4$. Indeed, as discussed above in section 3.2, this behaviour is dominated by a characteristic universal square-root edge singularity, independent of the underlying disorder distribution. In figure 4(*a*), we focus on the edge singularity, highlighting our findings for the two waiting time distributions. A scaling plot is shown, meant to elicit the power-law behaviour as $\phi \to \pi/4$. The full lines represent the exact formulae following from equation (8). Small deviations near the edge (large negative abscissa), which were not previously visible in figure 3(*a*), are now readily apparent, arising as a lattice artefact missed by our continuum result. A quick fit to the simulation data reveals a slope that is 10% too large. Surprisingly, even the exact curves have a slope that is too big, ≈ 0.52 or so. An examination of the effective exponent, see figure 4(*b*), clarifies the situation, showing that the true square-root singularity is rather stubborn and manifests itself only very, very close to the edge. For simulations of the DPRM on a discrete square lattice, this will require an extremely large system size, in order that the first site off the edge possesses an angular location $\phi \approx \pi/4 - e^{-15}$, not an easy task.

5. The point-to-line problem

So far we have considered directed polymers pinned at both ends; in the thermodynamic limit $L \to \infty$ this also fixes the orientation ϕ. Alternatively, one may fix only one endpoint and let the other end of the polymer lie anywhere on a straight 'substrate' line forming some angle θ relative to the x-axis (figure 5). In the context of first-passage percolation [13], which is an equivalent formulation of the DPRM problem [14], this is known as the *point-to-line* geometry. In the thermodynamic limit a particular orientation $\phi(\theta)$ is then chosen by minimizing (or maximizing) the energy among all allowed orientations. The point-to-line geometry appears naturally [19] when the dynamics of growing interfaces is formulated in terms of directed polymers [7].

5.1. The Wulff construction

By translational invariance the point-to-line problem is equivalent to the line-to-line problem, in which the optimal path connecting two parallel lines, both at an angle θ with the x-axis, is to be determined. The optimal path energy, divided by the distance l between the lines (equivalently, the width of the 'strip' enclosed by the two lines, see figure 5), will be denoted by $\tilde{e}_{\min}(\theta)$ and $\tilde{e}_{\max}(\theta)$ for the minimum and maximum energy case, respectively. As can be seen from this figure, the length of a polymer oriented at an angle ϕ is $l/\cos(\phi - \theta)$, hence the quantity to be minimized (maximized) with respect to ϕ is $e_{\min}(\phi)/\cos(\phi - \theta)$ ($e_{\max}(\phi)/\cos(\phi - \theta)$), and we have

$$\tilde{e}_{\min}(\theta) = \min_{\phi} \left(\frac{e_{\min}(\phi)}{\cos(\phi - \theta)} \right) \tag{26}$$

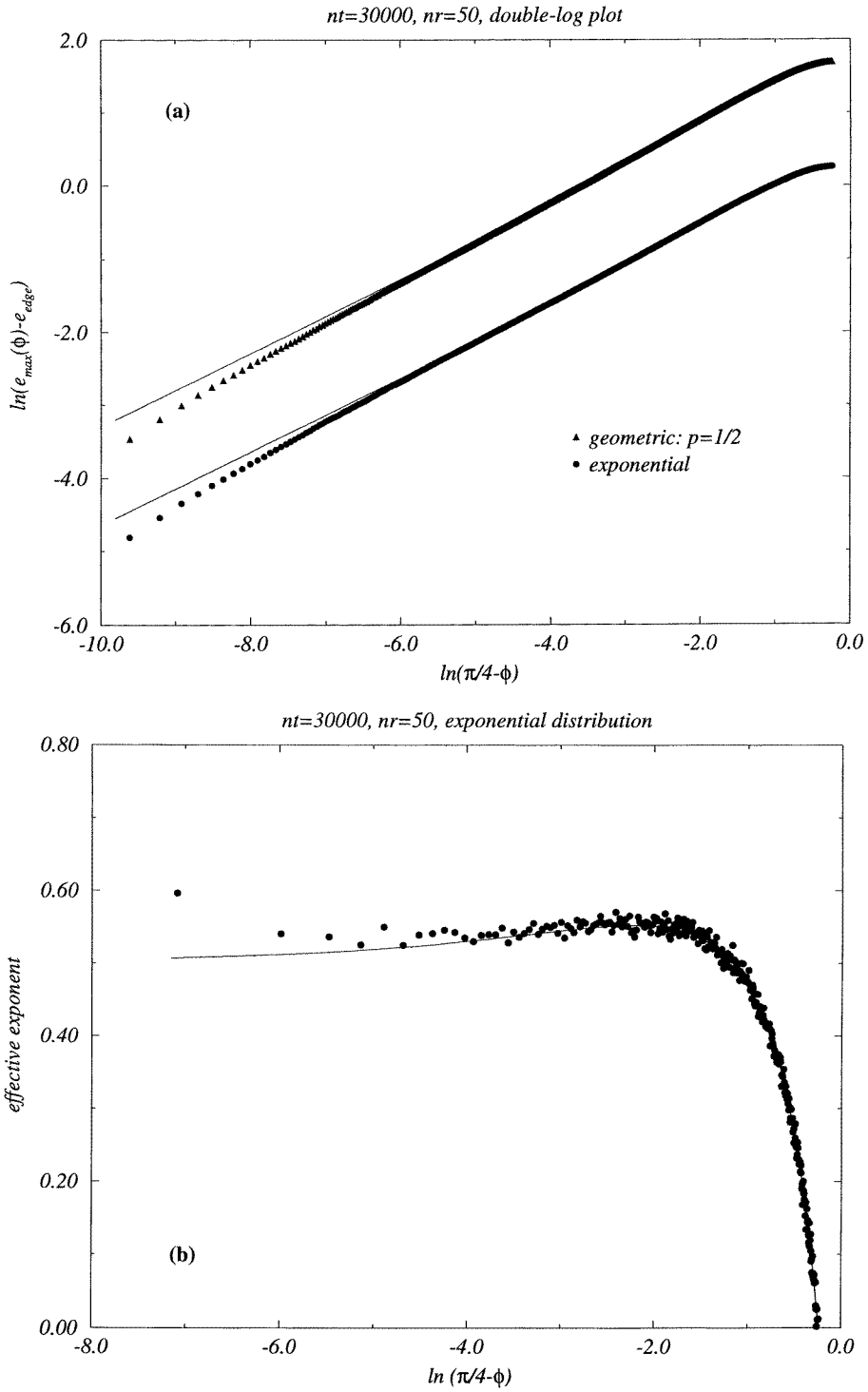

Figure 4. (*a*) Edge singularity for two waiting time distributions. Here, $e_{\text{edge}} = \bar{\epsilon}/\sqrt{2}$. (*b*) Corresponding effective exponent for the case of the exponential distribution. Note that the full curves represent exact results, not least-squares fits, while the symbols indicate simulation data.

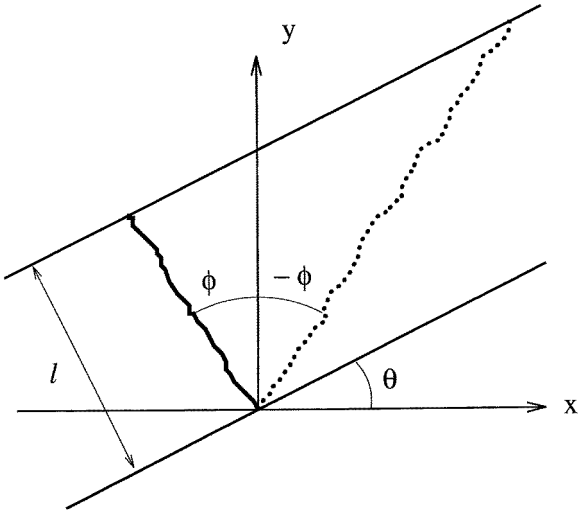

Figure 5. Geometry of the point-to-line optimization problem, showing the substrate inclination angle θ, as well as the terminal navigation direction ϕ. The dotted polymer conformation illustrates the symmetry argument used in the derivation of equation (31).

$$\tilde{e}_{\max}(\theta) = \max_{\phi} \left(\frac{e_{\max}(\phi)}{\cos(\phi - \theta)} \right). \tag{27}$$

The reader may have recognized that equation (26) is precisely the two-dimensional Wulff construction [25] for the minimal energy shape of a domain with line tension $e_{\min}(\phi)$. The point-to-line energy $\tilde{e}_{\min}(\theta)$ is therefore obtained from the following geometric procedure: For each angle ϕ, a ray of length $e_{\min}(\phi)$ is drawn from the origin, and a straight line running through its endpoint is constructed perpendicular to the ray. Then the function $\tilde{e}_{\min}(\theta)$ is the inner envelope of these lines. Similarly $\tilde{e}_{\max}(\theta)$ is the outer envelope of lines constructed from the polar plot of $e_{\max}(\phi)$.

5.2. The optimal path angle

The orientation selected by the directed polymer in the point-to-line geometry is given by the angle $\phi_{\min,\max}(\theta)$ at which the optimum in equations (26) and (27) is attained. As a first illustration, consider the case without disorder, where the minimum (maximum) energy path is simply the path with the minimum (maximum) number of bonds. For $\theta = 0$ all paths traverse the same number of bonds. However, for any $\theta > 0$ it is easy to see that the minimum energy path follows the lattice diagonal $(1, -1)$, while the maximum energy path runs along the $(1, 1)$ direction; for $\theta < 0$ their roles are reversed. Thus we have

$$\phi_{\min,\max} = \begin{cases} \pm\pi/4 & \theta > 0 \\ \mp\pi/4 & \theta < 0. \end{cases} \tag{28}$$

In the absence of disorder $e_{\min}(\phi) = e_{\max}(\phi) = \bar{\epsilon}\cos\phi$, hence by inserting (28) into the general expressions (26) and (27) we find

$$\tilde{e}_{\min}(\theta) = \frac{\bar{\epsilon}}{\cos\theta + |\sin\theta|} \tag{29}$$

corresponding to a domain shape with facets at $\theta = \pm\pi/4$, and

$$\tilde{e}_{\max}(\theta) = \frac{\bar{\epsilon}}{\cos\theta - |\sin\theta|}. \tag{30}$$

We shall see later that the divergence of $\tilde{e}_{\max}$ at $\theta = \pm\pi/4$ is a generic feature.

Some properties of the optimal path angle in the presence of disorder can be proved in generality. Owing to the symmetry under $\theta \to -\theta$ we may restrict ourselves to the range $\theta \geqslant 0$. Then

$$\phi_{\min}(\theta) \geqslant 0 \qquad \phi_{\max}(\theta) \leqslant 0 \qquad (0 \leqslant \theta \leqslant \pi/4). \tag{31}$$

To see this, suppose that for some angle $\theta > 0$, $\phi_{\min}(\theta) = \phi_0 < 0$. Since $e_{\min}(\phi)$ is symmetric around $\phi = 0$, the path with orientation $-\phi_0 > 0$ has the same energy per unit length but is shorter (figure 5), thus contradicting the assumption. The statement that $\phi_{\max} \leqslant 0$ follows in the same way.

Next we show that

$$\lim_{\theta\to\pi/4} \phi_{\max}(\theta) = -\pi/4. \tag{32}$$

This is equivalent to the statement that $\tilde{e}_{\max}$ diverges at $\theta = \pi/4$. The latter follows from the observation that $\tilde{e}_{\max}(\theta)$ is bounded from below by the energy of the 'edge' path at $\phi = -\pi/4$, which is given by $\bar{\epsilon}/\sqrt{2}\cos(\theta + \pi/4)$ and diverges as $\theta \to \pi/4$. In this limit, the optimal path can increase its length without bounds by aligning with the substrate.

To proceed, we assume that $e_{\min,\max}$ are smooth functions of ϕ. The optimal path angle is then found by equating the derivative of $e_{\min,\max}(\phi)/\cos(\theta - \phi)$ with respect to ϕ, to zero. This yields

$$\tan(\theta - \phi_{\mathrm{m}}) = \frac{e'_{\mathrm{m}}}{e_{\mathrm{m}}} \tag{33}$$

where we use e_{m}, ϕ_{m} as a shorthand for $e_{\min,\max}$, $\phi_{\min,\max}$ in relations which hold both for the minimum and maximum energy paths, and $e'_{\mathrm{m}} = \mathrm{d}e_{\mathrm{m}}/\mathrm{d}\phi$.

Consider first the case of small θ. At $\theta = 0$, $\phi_{\min} = \phi_{\max} = 0 = \theta$ by symmetry. Expanding equation (33) near $\theta = \phi = 0$ we obtain

$$\phi_{\mathrm{m}} \approx \frac{e_{\mathrm{m}}(0)}{e_{\mathrm{m}}(0) + e''_{\mathrm{m}}(0)}\theta. \tag{34}$$

For small angles ϕ_{m} is linear in θ, with a prefactor inversely proportional to the 'stiffness' $e_{\mathrm{m}}(0) + e''_{\mathrm{m}}(0)$. The inequalities (31) yield a definite sign for the stiffnesses,

$$e_{\min}(0) + e''_{\min}(0) \geqslant 0 \qquad e_{\max}(0) + e''_{\max}(0) \leqslant 0. \tag{35}$$

For the exponential and geometric distributions equation (8) yields $e_{\max}(0) + e''_{\max}(0) = -\sigma$.

Through equation (33) the divergence of $\phi_{\max}$ for $\theta \to \pi/4$ is linked to the square-root edge singularity of $e_{\max}(\phi)$. Let $\theta = \pi/4 - \Delta\theta$ and $\phi_{\max} = -\pi/4 + \Delta\phi$, then equation (10) yields $e'_{\max}(\phi_{\max}) \sim (\Delta\phi)^{-1/2}$. Inserting this into (33) it follows that $\Delta\phi \sim (\Delta\theta)^2$, i.e. the optimal angle $\phi_{\max}$ approaches its limit (32) at zero slope. In contrast, the minimum energy angle $\phi_{\min}(\theta)$ approaches a nonuniversal limit $\phi^*_{\min} < \pi/4$ for $\theta \to \pi/4$, which is given by the solution of (33) with $\theta = \pi/4$.

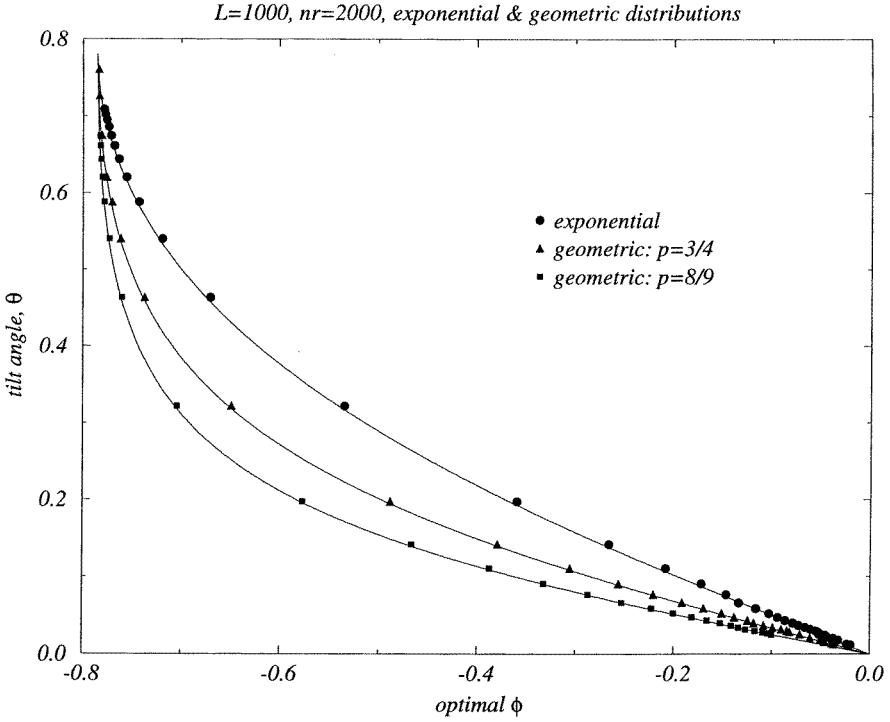

Figure 6. DPRM point-to-line problem: theory versus simulation for exponential and geometric distributions. Observe the linear response for small inclination angles, $\theta \to 0$.

5.3. Simulation of point-to-line paths

As a test of the above findings, we have studied a variant of the zero-temperature DPRM, adapted to the geometry previously indicated in figure 5. For $\theta \neq 0$, the shortest walks (i.e. those with $\phi = \pi/4$) possess 1000 steps. Disorder averages were performed over 2000 realizations of the random energy landscape. In the case of the exponential and geometrical distributions, our fundamental formula, equation (33), can be rewritten,

$$\theta = \phi - \tan^{-1}\left(\frac{\bar{\epsilon}\sin\phi + \sigma\sin 2\phi/\sqrt{\cos 2\phi}}{\bar{\epsilon}\cos\phi + \sigma\sqrt{\cos 2\phi}}\right) \tag{36}$$

which expresses the optimal navigation direction, ϕ, implicitly in terms of the substrate inclination angle θ. In figure 6, we show this theoretical curve, along with our numerical results. Clearly, the agreement is quite good. It should be noted that for small inclination angles, the response is *linear*. In fact, expansion of (33) in the limit $\theta \to 0$, reveals $\theta \approx -\phi/2$, the slope of $-\frac{1}{2}$ unique to this choice of an exponential disorder distribution; see, too, equation (34). Also included in this figure are the theoretical and numerical results for the geometric distribution for two distinct values of the parameter p. Here, we again find good agreement. In the small angle limit, it can be readily shown that the slope in the linear regime is equal to $-1/(1+\sqrt{1/(1-p)})$, which explains our selection of $p = \frac{3}{4}, \frac{8}{9}$ and is nicely reflected in the figure itself. As is apparent in all cases, the optimal navigation direction varies quite rapidly as the destination line inclination approaches $\pi/4$; i.e. as the wedge geometry becomes strongly skewed.

6. Conclusions

In this paper we have derived a number of properties of directed optimal paths in random media, some of which are specific to the underlying disorder distribution, such as equation (8), while others, e.g. equations (25), (32) and (35), are universally valid. A surprising result is the simplicity of the expression (8) for the maximum path energy in the case of exponential or geometric disorder. As was mentioned above, its derivation relies crucially on the Markovian nature of the underlying dynamical model, and therefore it is unlikely that comparably explicit results could be obtained for other distributions. Nevertheless it seems conceivable that equation (8) has some validity as an approximation, or possibly as a bound on $e_{\max}(\phi)$ in the general case also.

To conclude, we would like to point out a possible experimental realization of our work. There is considerable evidence that the DPRM provides a reasonable model for fracture lines in two dimensions, at least for quasistatic fracture of ductile materials [26–28]. An important example is the rupture of paper [29]. As a consequence of the fabrication procedure, machine-made paper is strongly anisotropic [30]. Applying the considerations of section 5.2, we therefore expect that a strip of paper which is cut at some angle θ relative to the direction of minimal or maximal strength will rupture along a line which forms some nontrivial angle $\phi(\theta)$ with respect to the strip edges. Through the relation (33), systematic measurements of $\phi(\theta)$ would then provide information about the underlying strength anisotropy.

Acknowledgments

JK is most grateful to Timo Seppäläinen for helpful remarks and to IMPA, Rio de Janeiro, and MPI für Physik komplexer Systeme, Dresden, for their hospitality. TH-H is grateful for NSF DMR-9528071, Condensed Matter Theory, as well as a productive early winter visit to Essen, Duisburg, and Düsseldorf. Finally, this work was supported by NATO within CRG.960662.

References

[1] Wulff G 1901 *Z. Kristallogr.* **34** 449
[2] Rottman C and Wortis M 1984 *Phys. Rep.* **103** 59
[3] Rottman C and Wortis M 1981 *Phys. Rev.* B **24** 6274
[4] Forgacs G, Lipowsky R and Nieuwenhuizen Th M 1991 *Phase Transitions and Critical Phenomena* vol 14, ed C Domb and J L Lebowitz (London: Academic)
[5] Huse D S and Henley C L 1985 *Phys. Rev. Lett.* **54** 2708
[6] Kardar M and Zhang Y C 1987 *Phys. Rev. Lett.* **58** 2087
[7] Kardar M, Parisi G and Zhang Y C 1986 *Phys. Rev. Lett.* **56** 889
[8] Halpin-Healy T J and Zhang Y C 1995 *Phys. Rep.* **254** 215
[9] Alava M J and Duxbury P M 1996 *Phys. Rev.* B **54** 14 990
[10] Essam J W, Guttmann A J and De'Bell K 1988 *J. Phys. A: Math. Gen.* **21** 3815
[11] Richardson D 1973 *Proc. Camb. Phil. Soc.* **74** 515
[12] Rost H 1981 *Z. Wahrscheinlichkeitstheorie Verwandte Geb.* **58** 41
[13] Kesten H 1986 *École d'Été de Probabilités de Saint Flour XIV-1984 (Springer Lecture Notes in Mathematics 1180)* ed R Carmona, H Kesten and J B Walsh (Berlin: Springer) p 126
[14] Krug J and Spohn H 1991 *Solids Far From Equilibrium* ed C Godrèche (Cambridge: Cambridge University Press) p 479
[15] Tang L-H 1992 *Growth Patterns in Physical Sciences and Biology* ed E Louis, L M Sander, P Meakin and J M Garcia-Ruiz (New York: Plenum)
[16] Krug J and Tang L-H 1994 *Phys. Rev.* E **50** 104

[17] Meakin P, Ramanlal P, Sander L M and Ball R C 1986 *Phys. Rev.* A **34** 5091
[18] Derrida B, Evans M, Hakim V and Pasquier V 1993 *J. Phys. A: Math. Gen.* **26** 1493
[19] Krug J, Meakin P and Halpin-Healy T 1992 *Phys. Rev.* A **45** 638
[20] Yaguchi H 1986 *Hiroshima Math. J.* **16** 449
[21] Schadschneider A and Schreckenberg M 1993 *J. Phys. A: Math. Gen.* **26** L679
Schadschneider A and Schreckenberg M 1997 *J. Phys. A: Math. Gen.* **30** L69
[22] Glynn P W and Whitt W 1991 *Ann. Appl. Prob.* **1** 546
[23] Seppäläinen T 1997 *Ann. Appl. Prob.* **7** 855
[24] Adler R J 1981 *The Geometry of Random Fields* (New York: Wiley)
[25] Nozières P 1991 *Solids Far From Equilibrium* ed C Godrèche (Cambridge: Cambridge University Press)
[26] Hansen A, Hinrichsen E L and Roux S 1991 *Phys. Rev. Lett.* **66** 2476
Lely D and Roux S 1991 *J. Physique* III **1** 1675
[27] Räisänen V I, Seppala E T, Alava M J and Duxbury P M 1998 *Phys. Rev. Lett.* **80** 329
[28] Bouchaud E 1997 *J. Phys.: Condens. Matter* **9** 4319
[29] Kertész J, Horváth V K and Weber F 1993 *Fractals* **1** 67
[30] Deng M and Dodson C T J 1994 *Paper: An Engineered Stochastic Structure* (Atlanta, FL: Tappi)